Mode 2 waves on the continental shelf: Ephemeral components of the nonlinear internal wavefield

E. L. Shroyer,[1,2] J. N. Moum,[1] and J. D. Nash[1]

[1]   Shoreward propagating, mode 2 nonlinear waves appear sporadically in mooring records obtained off the coast of New Jersey in the summer of 2006. Individual mode 2 packets were tracked between two moorings separated by 1 km; however, packets could not be tracked between moorings separated by greater distances from one another (~10 km). The inability to track individual packets large distances through the mooring array combined with detailed observations from a ship suggest that these waves are short lived. The evolution of the ship-tracked wave group was recorded using acoustic backscatter, acoustic Doppler current profilers, and turbulence profiling. The leading mode 2 wave quickly changed form and developed a tail of short, small-amplitude mode 1 waves. The wavelength of the mode 1 oscillations agreed with that expected for a copropagating tail on the basis of linear theory. Turbulent dissipation in the mixed layer and radiation of the short mode 1 waves contributed to rapid energy loss in the leading mode 2 wave, consistent with the observed decay rate and short life span of only a few hours. The energy in the leading mode 2 wave was 10–100 times smaller than the energy of mode 1 nonlinear internal waves observed during the experiment; however, the magnitudes of wave-localized turbulent dissipation were similar.

1.   Introduction

[2]   Nonlinear internal waves (NLIWs) are commonly seen in the coastal ocean. The bulk of observations consist of waves of depression, perhaps because of the relative ease of distinguishing these features using remote imagery [*Jackson*, 2004]. However, several studies also document waves of elevation [e.g., *Liu et al.*, 1998; *Klymak and Moum*, 2003; *Orr and Mignerey*, 2003; *Scotti and Pineda*, 2004; *Moum and Smyth*, 2006]. The terms, NLIWs of depression and elevation, automatically imply a mode 1 structure, in which all isopycnals are displaced in the same direction. Mode 2 nonlinear internal waves have also been observed in the ocean [*Farmer and Smith*, 1980; *Akylas and Grimshaw*, 1992, Figure 2; *Duda et al.*, 2004; *Bogucki et al.*, 2005; *Yang et al.*, 2009] and in the laboratory [*Davis and Acrivos*, 1967; *Helfrich and Melville*, 1986; *Hüttemann and Hutter*, 2001; *Mehta et al.*, 2002]. These higher-mode waves are of two types. Either upper isopycnals are displaced upward and lower isopycnals are

displaced downward, or the opposite is true. The first type of mode 2 wave is sometimes referred to as varicose, emphasizing the bulging shape; the observations presented here are of this type.

[3]   Several studies highlight potential mechanisms for the formation of mode 2 NLIWs. For example, *Helfrich and Melville* [1986] found that a mode 2 wave may emerge after a shoaling first baroclinic mode wave undergoes a breaking instability, while *Hüttemann and Hutter* [2001] and *Vlasenko and Hutter* [2001] describe the formation of reflected and transmitted mode 2 waves after a mode 1 wave encounters a sill. A separate modeling study generated mode 2 waves via resonant interaction of a depth-independent velocity field with topography, where the background velocity was set near the mode 2 linear wave speed [*Stastna and Peltier*, 2005]. These first three examples involve differing topographic interactions, which may not always be necessary. Both *Maxworthy* [1980] and *Mehta et al.* [2002] produced mode 2 waves at the head of gravity intrusions in lab studies.

[4]   Theoretical studies and numerical models have been employed to study the structure and form of mode 2 nonlinear waves [*Davis and Acrivos*, 1967; *Tung et al.*, 1982; *Akylas and Grimshaw*, 1992; *Vanden-Broeck and Turner*, 1992; *Stastna and Peltier*, 2005]. A noteworthy characteristic of mode 2 waves is the development of an oscillatory wave tail, which consists of a series of short, linear mode 1 waves. Mode 2 waves are not unique in this respect, and, in theory, a leading nonlinear wave of arbitrary mode number

[1]College of Oceanic and Atmospheric Sciences, Oregon State University, Corvallis, Oregon, USA.
[2]Now at Woods Hole Oceanographic Institution, Woods Hole, Massachusetts, USA.

greater than 1 may develop a tail composed of lower-mode waves [*Akylas and Grimshaw*, 1992]. The growth of the tail is related to wave speed dependence on vertical mode number and horizontal wavelength. For example, consider again the case of a mode 2 nonlinear wave. Since internal wave speed increases with wavelength and decreases with mode number, short mode 1 waves may travel at the same speed as long mode 2 waves for a given background state. The resonance condition, at which the short mode 1 wave speed is equal to the wave speed of the long mode 2 wave (i.e., $c_1 = c'_2$, where c_1 is the linear, first baroclinic mode wave speed and c'_2 is the nonlinear mode 2 speed), results in copropagation of waveforms and permits growth of the oscillatory mode 1 wave tail. This growth comes at the expense of the nonlinear wave's energy. In the previous relationship, the wave speed of the mode 2 wave is distinguished from the wave speed of the short mode 1 tail with the appropriate subscripts. Measured, nonlinear wave speeds are primed.

[5] While the mode 2 wave with its tail is not a soliton in the strict definition as it is neither steady (radiative loss to the wave tail) nor solitary, the waveform is sometimes referred to as a weakly nonlocal solitary wave or generalized solitary wave [e.g., *Boyd*, 1990; *Vanden-Broeck and Turner*, 1992]. These terms are not limited to mode 2 internal waves as generalized solitary wave solutions exist for equations governing gravity-capillary solitary waves [*Hunter and Vanden-Broeck*, 1983] and nonlinear Rossby waves [*Williams and Wilson*, 1988]. The development of a resonant tail is distinct from transient, dispersive wave tails, which may form as a wave evolves, in that the tail and NLIW travel at the same speed (i.e., copropagate). The observations presented here show a mode 1 wave tail that forms after the first sighting of the mode 2 wave group, and, as such, there is some question as to whether the observed tail is an artifact of resonance or dispersion.

[6] In this paper we investigate mooring- and ship-based observations of mode 2 waves recorded during the Office of Naval Research's Nonlinear Internal Wave Initiative–Shallow Water '06 experiment (NLIWI-SW06) on the New Jersey shelf. This paper begins with a review of the experiment in section 2, followed by a description of the observed waves in section 3. The structure and energetics of the ship-based observations are detailed in sections 4 and 5, respectively. Possible generation mechanisms are discussed in section 6, followed by a summary (section 7). To aid the reader, we point out a subtlety of the terminology used in this manuscript. Mode 2 nonlinear waves are occasionally compared to other nonlinear, long mode 1 waves that were documented during SW06. These mode 1 NLIWs are distinct from the short, linear mode 1 waves that comprise the tail. Care was taken to refer to these waves as large amplitude or nonlinear, and, hopefully, the distinction between theses two types of mode 1 waves will be clear to the reader.

2. Experimental Details

[7] As part of NLIWI-SW06 [*Tang et al.*, 2007], a shipboard survey of New Jersey's nonlinear wavefield was conducted in August 2006. The R/V *Oceanus* was equipped with a 120 kHz echo sounder, a side-mounted RD Instru-

ments (RDI) 1200 kHz acoustic Doppler current profiler (ADCP), and a hull-mounted RDI 300 kHz ADCP. These shipboard acoustics, combined with the ship's X band radar and visual sightings, were used to locate and track shoreward propagating wave groups. Wave groups were transited through at $3–4 \text{ m s}^{-1}$ from the back to the leading wave, at which point the ship was turned and held stationary. As the wave propagated past the ship, microstructure measurements (density and turbulent dissipation) were collected using the Chameleon profiler [*Moum et al.*, 1995]. Typically, the first three to four waves passed the ship before the ship was turned and the process was repeated. Shipboard observations of 27 wave groups were obtained. One particular wave group consisted of mode 2 waves, the focus of this analysis.

[8] The shipboard survey coincided with a large-scale mooring deployment. Two environmental moorings, SW30 and SW38, were located 1 km apart near the 80 m isobath (Figure 1), and eight groups of mode 2 waves were identified in these mooring records over the course of a month. SW30 was a water column mooring equipped to measure both density and velocity with conductivity-temperature-depth (CTD) sensors located at 14, 17, 21, 26, 33, 40, 48, 57, 66, and 75 m and upward facing ADCP sampling 4 m vertical bins every 30 s. SW38 was a bottom lander with an upward facing RDI 300 kHz ADCP that sampled 1 m bins every 5 s. Lower-frequency mode 2 oscillations were evident in the velocity record at the nearest offshore mooring (SW41), but we could not distinguish any mode 2 NLIWs in this record. The nearest onshore mooring (SW37, located 10 km inshore of SW30) was a bottom lander similar in setup to SW38. No mode 2 waves were identified in its velocity record. The nearest onshore water column temperature sensors (located at 1, 12, 21, 31, 42, 55, and 60 m) were on SW29, which was positioned 20 km inshore of SW30 along the mooring line. (Note that SW29 is not shown in Figure 1.) From this temperature record, only two sets of mode 2 waves were isolated. SW29 was also equipped with a bottom-mounted ADCP that sampled the water column with a setup identical to SW30.

3. Observations

3.1. Mooring Record

[9] Mode 2 wave trains were discernible in the temperature and velocity data recorded at mooring SW30 (located at the x-y origin in Figure 1). While the nearby bottom lander, SW38, was equipped to better resolve water column velocities, distinguishing mode 2 waves from the record is difficult because of sidelobe contamination of near-surface velocity data and energetic background shear. Therefore, we rely on the temperature record at SW30 to identify mode 2 waves and then project these times backward to help identify the mode 2 waves in the SW38 velocity record. Mode 2 wave properties at these two moorings are summarized in Table 1. The fourth group was observed at SW30 but not in the SW38 record.

[10] Ideally, wave amplitudes should be calculated using maximum displacements, but the limited vertical resolution of the mooring CTD data precludes such an approach. Instead, amplitudes (A) were calculated in the following
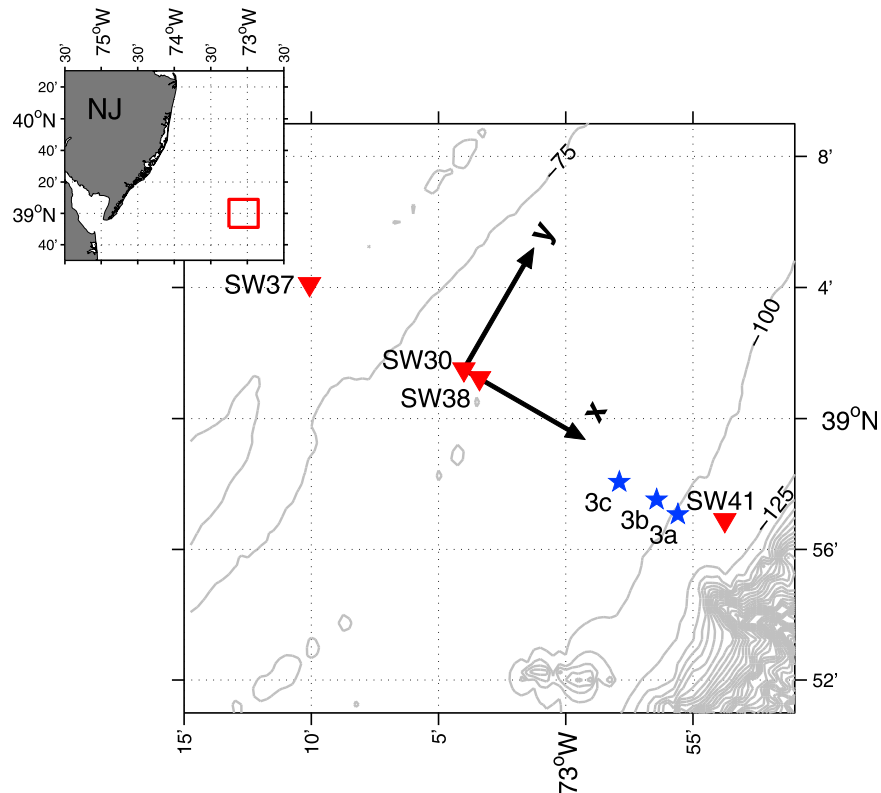
Figure 1. SW06 site and bathymetry. Moorings, SW38 and SW30, that were used in this analysis are shown along with the two nearest across-shelf environmental moorings, SW37 and SW41 (red triangles). SW29 (not shown) is located 10 km inshore of SW37 along the same mooring line. The blue stars indicate locations of shipboard profiling series through Wave Jasmine, with reference to Figures 3a–3c; the black axes define the coordinate system.

manner. First, temperature records were converted to displacements (η) using the relation

$$\eta = \frac{\theta'}{\partial \theta / \partial z}$$

at sensors located at 14 and 26 m depths. Here θ' is the perturbation temperature and $\overline{\partial \theta / \partial z}$ is a time-averaged, vertical gradient of temperature at each sensor. The time average was computed over 90 min surrounding the mode 2 wave trains. The 14 m sensor provided the closest available measurement to the surface. In all but one case, this upper sensor recorded upward displacements, and the lower sensor recorded downward displacements through mode 2 waves. The amplitude was then computed as $A = 1/2 \, (|\eta_{14 \, m}| + |\eta_{26 \, m}|)$. For the eighth wave group, the 14 m sensor only recorded upward displacements in the leading wave. The $\eta_{14 \, m}$ value of the trailing waves was negligible, indicating that the sensor was possibly in the middle of the pycnocline. The amplitude in these waves was assumed to be equal to $A = |\eta_{26 \, m}|$. The wave period, T, was then calculated as the amount of time that $\eta_{14 \, m}$ ($\eta_{26 \, m}$) was greater (less) than zero through each disturbance.

[11] Wave headings are given in degrees clockwise from north. The wave heading was calculated by assuming that (1) the variance of the high-passed velocity (filtered at 30 min) in the along-crest dimension should be minimized and (2) the velocity in the core of the wave (i.e., the middle layer for the mode 2 waves) should be positive. The velocity data acquired through each wave train were rotated in 5° increments until these conditions were met. Since the variance of high-passed velocity was dominated by the wave signal, the first condition minimizes the wave velocity signal in the along-crest direction. By itself, this criterion results in two possibilities separated by 180°; the second condition then selects the direction consistent with a positive wave particle velocity, so that the wave particle velocity is in the same direction as the wave speed as opposed to opposite the wave speed. Note that in calculating the wave heading, the reference frames used, i.e., the wave's reference frame and the cardinal directions, are distinct from that shown in Figure 1. However, all mode 2 wave groups propagated within ±20° of the negative x axis shown in Figure 1.

[12] The observed mode 2 wave speeds, c'_2, were calculated as $c'_2 = \Delta x \cos(\delta\phi)/\Delta t$, where $\delta\phi$ is the angle between the wave heading and the mooring line, Δx is the distance between SW38 and SW30, and Δt is the difference in the leading wave's arrival time at the moorings. Note that c'_2 includes advection by the background current. In contrast to the convention used for measured velocities (with negative u directed onshore), positive values of c'_2 are directed shoreward. In an attempt to adjust for advection, the depth mean current in the direction of wave propagation at SW30 was averaged for the hour preceding wave arrival to estimate a

Table 1. Summary of Mode 2 NLIW Properties as Observed From Moorings SW38 and SW30[a]

Time[b]	A (m)	T (min)	c'_2	c^*_2	Heading (deg)
Observation 1					
1732 UTC 2 August 2006	5.7	10.4	0.35	0.28	320
1817 UTC 2 August 2006	6.2	10.4			
	6.6	9.5			
Observation 2					
1444 UTC 3 August 2006	4.0	5.5	0.44	0.37	315
1520 UTC 3 August 2006	4.4	5.8			
	3.7	7.6			
	4.5	6.1			
	5.8	4.5			
	4.1	3.9			
Observation 3					
0232 UTC 16 August 2006	5.3	6.8	0.47	0.39	280
0305 UTC 16 August 2006	3.8	6.7			
	3.4	5.9			
	3.1	5.1			
	1.6	3.6			
Observation 4					
No Signal	3.0	5.9			290
1610 UTC 17 August 2006	2.6	5.1			
Observation 5					
1842 UTC 20 August 2006	3.2	11.5	0.37	0.29	300
1926 UTC 20 August 2006	3.5	7.4			
	3.0	6.7			
Observation 6					
2333 UTC 20 August 2006	2.3	9.6	0.31	0.37	295
0025 UTC 21 August 2006	4.7	10.5			
Observation 7					
1251 UTC 22 August 2006	1.9	12.9	0.23	0.38	295
1404 UTC 22 August 2006	3.0	11.1			
	5.5	8.0			
	3.6	10.2			
	2.9	11.8			
Observation 8					
1338 UTC 29 August 2006	7.5	11.5	0.45	0.40	290
1414 UTC 29 August 2006	3.3	13.5			
	5.5	6.9			
	5.7	9.8			

[a]The amplitude, A, and period, T, are defined in section 3. Wave speeds, c'_2, are calculated by differencing arrival times at SW38 and SW30. The value c^*_2 is adjusted for advection by barotropic currents (calculated as an hour-long average of the depth-mean velocity immediately preceding the arrival of each wave.)

[b]First time is arrival at SW38; second time is arrival at SW30.

barotropic velocity ($\overline{u_0}$). The corrected wave speeds were then calculated as $c^*_2 = c'_2 + \overline{u_0}$. The addition sign is needed since the conventions for the wave speed and water column velocity differ. Note that $\overline{u_0}$ is an approximation to the depth mean current since the upper 10 m of the water column were not resolved. Thus, caution should be exercised in seeking a relation between the amplitude and wave speed, as would be expected from weakly nonlinear theory, because of uncertainty in c^*_2.

[13] Mode 2 wave groups detected at SW30 and SW38 were composed of two to six waves. Lower-mode tails were not observed in the mooring records, a possible result of a relatively coarse sampling scheme. A varied from 1.6 to 7.5 m, with an average of 4.1 m; the distribution of A is shown in Figure 2a. These magnitudes are similar to those obtained from full-depth density profiles for the ship-tracked wave group presented in section 3.2. T was, on average, 8 min, but the distribution was bimodal (Figure 2b). Shorter wave periods, which occurred in wave groups 2–4, are centered around 6 min, and larger values of T, which were found for wave groups 1 and 5–8, are centered around 10 min. The average c_2 is 0.38 m s^{-1} with a propagation direction of 300°. The average c^*_2 is 0.35 m s^{-1}, with five measurements near 0.4 m s^{-1} and two just under 0.3 m s^{-1}. Arrival times of the mode 2 waves were not clearly linked to the M$_2$ barotropic tide, which was calculated using a harmonic fit to velocity data. Arrival times relative to the peak ebb varied from 5.7 h to just under 12 h, and arrival times relative to the previous mode 1 wave group show an even larger spread with time lags from 2.5 to 12.5 h.

[14] Two additional mode 2 wave groups were recorded in the temperature and velocity records at SW29, located inshore another 20 km from SW30. Both groups propagated onshore at 300°. The first, which was observed at 1400 UTC on 7 August 2006, propagated into a strong offshore flow whose magnitude was approximately equal to the onshore wave particle velocities (~0.15 m s^{-1}). This wave group consisted of a large leading wave ($T = 10$ min, $A = 7$ m) and
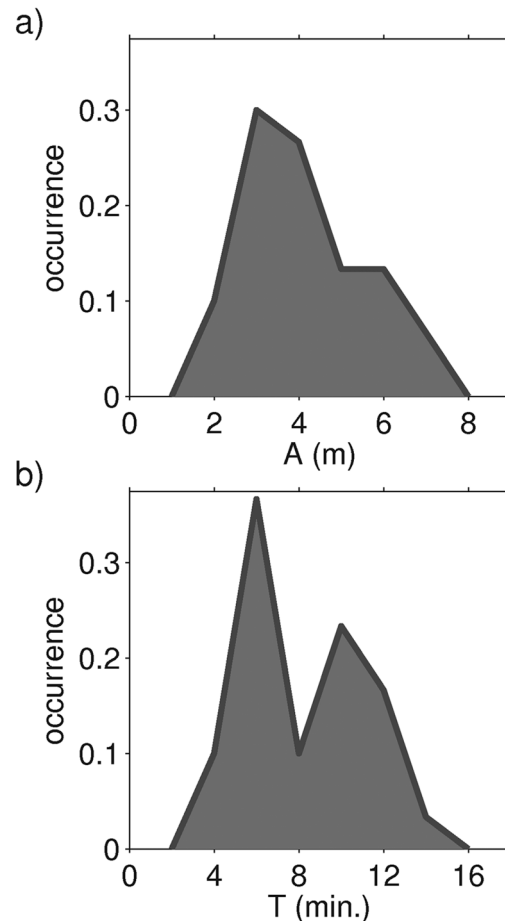
Figure 2. The distributions of (a) A and (b) T for mooring-observed waves.

a weak trailing wave with amplitudes and particle velocities less than half of the leading wave. The second wave group was observed at 0925 UTC on 26 August 2006 and consisted of four mode 2 waves with periods near 5 min and amplitudes ranging from 3 to 7 m. Neither of these wave groups were apparent in the records from SW30 and SW38. Amplitudes and periods were calculated as described above for SW30 but using sensors located at 12 and 31 m depth. Observed wave speeds were not calculated for the SW29 waves since these waves could not be identified in other mooring records.

[15] While small in number, at least two relevant conclusions can be drawn from these mooring observations. First, wave packets could not be tracked large distances through the mooring array, and in one case a wave packet that was observed in SW30 was not apparent just 1 km farther offshore in the record of SW38. Not only were mode 2 waves distinct from one another in the records of SW30 and SW29, which were separated by 20 km, but also, no mode 2 waves were observed in the SW37 record located midway between these two moorings. Therefore, an upward bound on the propagation distance of the mooring-observed mode 2 waves is likely 10 km. In contrast, larger-amplitude mode 1 waves were tracked large distances across the shelf (in some cases more than 40 km). The inability to track the mode 2 waves indicates that these waves were short lived in comparison to the large-amplitude mode 1 waves. Furthermore, the fact that some mode 2 packets were observed at inshore moorings but not at offshore moorings indicates that these waves are not formed in a well-defined location but instead may develop at multiple locations across the shelf. Second, mode 2 waves appeared irregularly with respect to both the M_2 tide and larger-amplitude mode 1 waves. This point combined with the nonspecific nature of a generation region hints that something other than the tide might play an important role in wave formation. However, the reader should note that during this experiment the large-amplitude mode 1 waves were not phased with the M_2 tide over most of the month, with 18–21 August being an exception. This property is in contrast to observations made by *Yang et al.* [2009] of summertime mode 2 waves in the South China Sea, which appeared at a roughly diurnal frequency and were likely related to tidal forcing. However, it is similar to the wintertime South China Sea mode 2 waves that also appeared randomly (albeit more frequently than New Jersey's mode 2 waves) [*Yang et al.*, 2009].

[16] Because of the limited number of mooring observations, sections 3.2, 4, and 5 are devoted to detailed analysis of an exemplary mode 2 wave group that was tracked by the ship. In particular, the ephemeral nature of mode 2 waves, which is alluded to in the mooring record by the inability to track the waves, is made more concrete by analysis of wave energetics for the ship-tracked wave group (section 5). In section 6, mooring records are again employed to facilitate a discussion on wave formation. Of special interest is the structure of the background fluid that was observed near the time of mode 2 wave occurrence.

3.2. Shipboard Record

[17] The mode 2 wave train, referred to as Wave Jasmine, was encountered at 2105 UTC on 11 August 2006 at 38.95°N, 72.92°W. (A naming convention was adopted for ship-tracked waves and is used here so that comparisons may be made with other SW06 NLIW papers.) Wave Jasmine was profiled through three times (Figure 1, stars) before the wave's signature was lost at 2315 UTC on 11 August 2006. Note that Jasmine was not observed at SW30, which is consistent with the loss of the shipboard signal 10 km farther offshore. Unlike most mode 1 depression waves, Jasmine initially lacked a clear surface signature (either visible or in X band radar). The wave group was tracked in the direction of wave propagation, 300°, calculated by minimizing the along-wavefront component of particle velocity. The direction coincided with the principal propagation direction of other large-amplitude mode 1 wave groups. Furthermore, a radar signature of the leading mode 2 waves was resolved for approximately 10 min in the final profiling transect. These images confirmed the chosen propagation direction. During the observation period, winds (as measured from the ship and corrected for ship motion) were from the southeast, roughly perpendicular to the direction of wave propagation. The wind speed decreased slightly from roughly 10 to 8 m s^{-1}. The winds and accompanying surface wave activity may have been sufficient to mask the signature of the mode 2 waves during the majority of the observation period, although further analysis, which is beyond the scope of this document, is required to fully understand the relationship between environmental conditions and the quality of X band return.

[18] During the first and second profiling periods, Jasmine consisted of three mode 2 waves (Figures 3a and 3b). In the third transect a sequence of relatively short mode 1 waves developed in the wakes of the first two mode 2 waves (Figure 3c). During this final transect, the bottom interface of the second wave was distorted, possibly as a consequence of the leading wave's tail, and the third mode 2 wave was no longer apparent. The wavelength (λ) of the leading wave decreased from about 180 to 120 m; in contrast, the shorter mode 1 waves had wavelengths near 60 m. The wavelength λ was defined using the acoustic backscatter images; although not shown here, note that the measured density displacements are consistent with the primary scattering surfaces of the mode 2 waves. The amplitude, defined by taking $(|\eta_{top}| + |\eta_{bot}|)/2$, where η_{top} (η_{bot}) is the maximum density displacement above (below) the pycnocline as measured from density profiles, was near 4 m in the first and final transect but slightly reduced to 3 m in the second transect. The small mode 1 waves were not resolved by the profiling scheme, and the amplitude of these waves is estimated as approximately 1 m, using the displacement from the midline to the peak outlined by the acoustic backscatter.

[19] Using the difference in distance and time between the three profiling periods, an average wave speed of $\overline{c'_2} = 0.48$ m s^{-1} is estimated. This value is slightly larger than the mode 2 linear phase speed, c_2, calculated using the Taylor-Goldstein (TG) equation with background shear [e.g., *Kundu and Cohen*, 2004]. The value of c_2 increased from 0.40 m s^{-1} at the first profiling site to 0.46 ms^{-1} at the third site. This increase was also observed in the local estimates of c'_2 and is attributed primarily to onshore advection by the barotropic current. Background profiles of $\rho_0(z)$ were estimated as averages of a minimum of two profiles taken ahead of the leading wave; background velocity profiles, $u_0(z)$, were calculated by averaging 10 min of data ahead of the
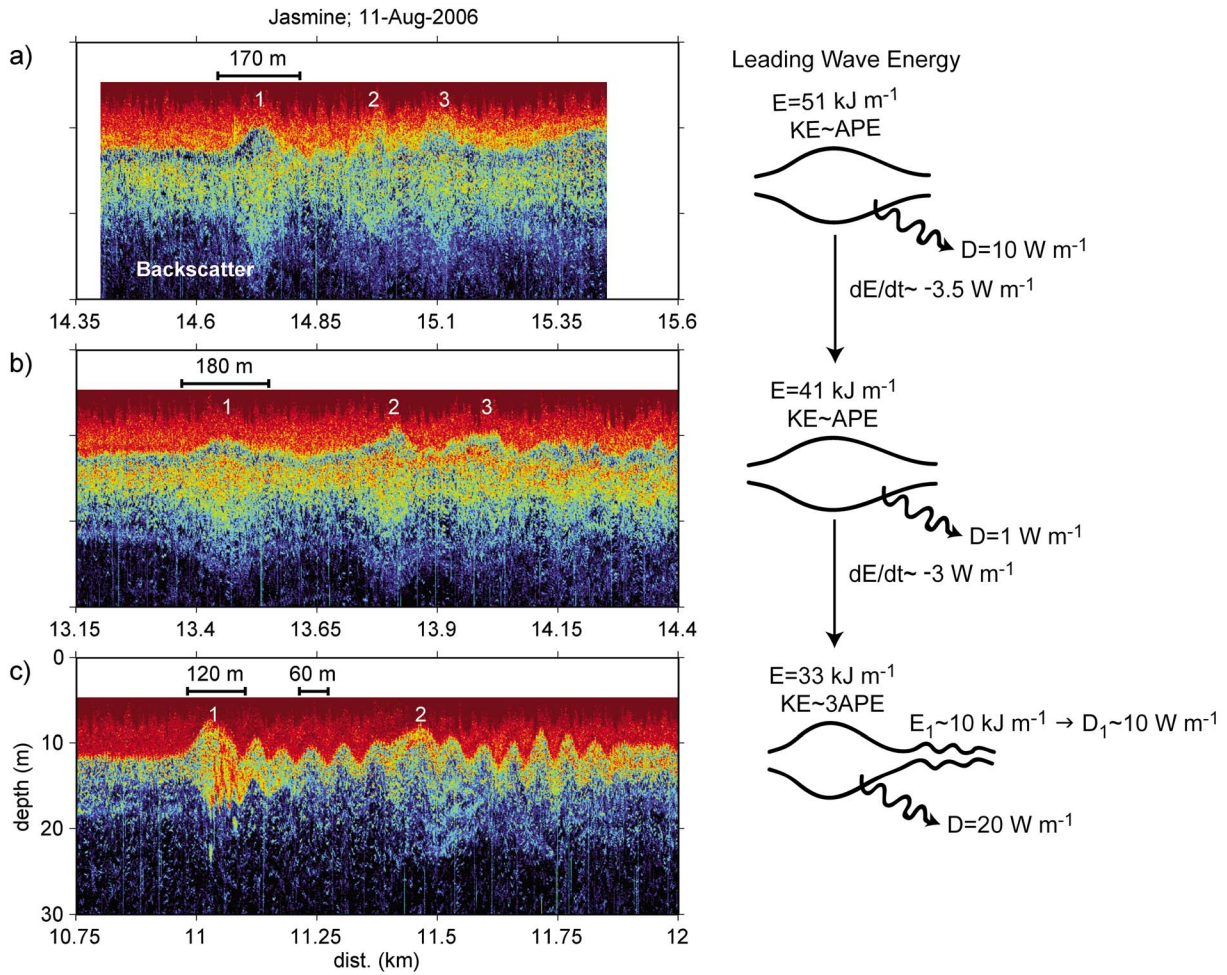
Figure 3. (left) Acoustic backscatter series for the (a) first, (b) second, and (c) third profiling series through Wave Jasmine. Time series have been converted to distances using the wave speed and the axes shown in Figure 1. Waves are propagating to the left. Distances are corrected for the Doppler shift using the ship velocity. (right) Schematic detailing lead wave energetics, which are discussed in section 5.

wave (Figure 4). Both $\rho_0(z)$ and $u_0(z)$ were low-pass filtered in the vertical with a cutoff wave number of 0.15 m^{-1}.

[20] The background density remained relatively steady during this period, although a general shift toward less dense water onshore existed. The pycnocline centered between ~10 and 20 m depth spanned two near-homogeneous layers located at the surface and at depth. While $u_0(z)$ maintained a consistent overall shape (e.g., the reversal at ~15 m), the exact structure and magnitude of the shear changed. For example, prior to the first crossing, the background velocity changed from −0.28 to 0.02 m s^{-1} in the upper 40 m, while $u_0(z)$ ahead of the third crossing decreased from approximately the same starting value to only −0.13 m s^{-1}. The nature of the background shear was quite complicated, particularly near the pycnocline, which corresponds to the vertical center of the mode 2 waves.

[21] The general characteristics of the mooring-observed mode 2 waves are consistent with those of Jasmine, discussed above. In addition, background profiles of salinity and velocity ahead of some mooring waves are similar to those observed for Jasmine; a more detailed analysis of the
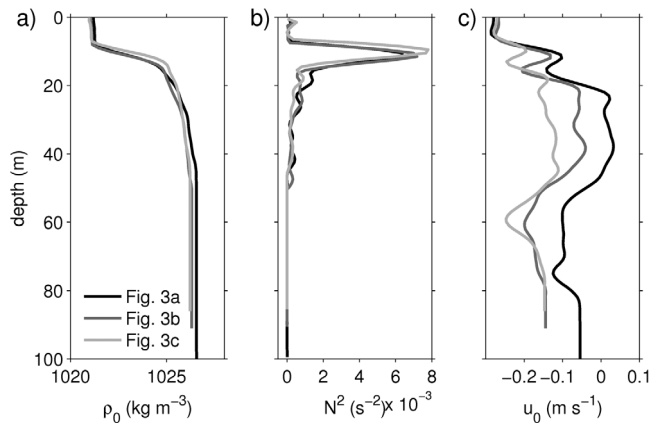

Figure 4. Background profiles of (a) density, (b) buoyancy frequency, and (c) velocity for the first, second, and third profiling series.
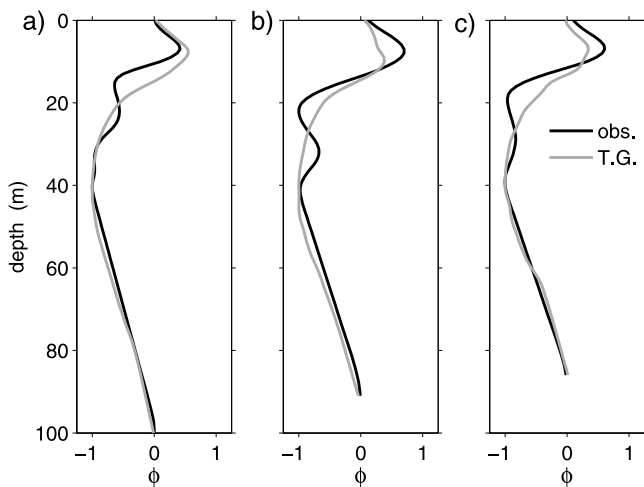
Figure 5. The observed vertical structure (black) and that calculated from the Taylor-Goldstein equation (grey) for the (a) first, (b) second, (c) and third profiling series for Wave Jasmine.

background fluid structure observed from moorings and the ship is given in section 6. However, first the structure and energetics of the leading wave in Jasmine are explored in sections 4 and 5. This extended analysis is possible for the ship-tracked group but not the mooring waves because of (1) the fine vertical resolution provided by Chameleon, (2) the fine horizontal resolution of the acoustic backscatter, and (3) the fact that Jasmine was sampled at multiple locations.

4. Wave Structure

4.1. Mode 2 Wave Structure

[22] The theoretical linear mode 2 structure function for vertical displacement, ϕ_{TG}, was computed from the TG equation using shipboard profiles of the background density, $\rho_0(z)$, and velocity, $u_0(z)$, upstream of the wave packet. This is compared to the observed vertical structure function, ϕ_{obs} (Figure 5), computed as the maximum wave-induced vertical displacements relative to the background state ρ_0 and normalized so that $\max(|\phi_{obs}|) = 1$. Densities were smoothed over 3 m bins prior to computing displacements. The value of ϕ_{obs} differs from that of ϕ_{TG}, particularly in the location of the maximum displacements in the final two transects. In the final transect, the upper and lower horizontal structures of the leading mode 2 wave were not symmetric (Figure 3c), and, consequently, are more reminiscent of work by *Stastna and Peltier* [2005] as opposed to modeling efforts which rely on a symmetry plane through the mixed layer [e.g., *Tung et al.*, 1982]. In particular, models that force a symmetrical response about the mixed layer do not allow for the development of a mode 1 wave tail.

4.2. Mode 1 Wave Tail

[23] Possibly the most striking feature of the shipboard observations is the sudden appearance of the mode 1 tail in the final transect (Figure 3c). The tail was fully formed by the time the ship ran back over the wave in between the profiling series shown in Figures 3b and 3c. Only 30 min

(~4.5*T*) passed between profiling through the leading wave at 13.4 km and the return transit. The change in wave structure, which was manifested in the decreased wavelength and the development of the short mode 1 tail, was coincident with changing conditions of the background fluid between the second and final series. A close examination of Figure 4 reveals an increase in stratification, a contraction of the pycnocline width that is also highlighted by a change in the backscatter return through the pycnocline (Figure 3), and a shallowing of the pycnocline. This final consideration is evidenced in the location of the stratification maximum in the final transect (Figure 4, light grey line), which is located a few meters closer to the surface than the maxima of the first two transects (Figure 4b). The waves thus propagated into a fluid with a shallower pycnocline that was "more" two-layer-like; that is, the peak stratification increased and the pycnocline width decreased slightly. Although subtle, this shift in the background conditions may be relevant to the onset of wave evolution. Since the tail was not observed at multiple locations, the growth of the wave tail could be a product of either transient dispersion or copropagation; we take this opportunity to highlight two aspects of the observations that suggest copropagation via the resonance condition.

[24] 1. The leading mode 2 waveform steepened. The decrease in λ between the second and third transect is significant and exceeds reasonable error bounds associated with the correction of the Doppler shift. Note that a reduction of wavelength is the opposite of what would be expected because of barotropic currents, since the wave propagated into a region of increased shoreward flow.

[25] 2. The tail is composed of oscillations of a single wavelength. To offer a more quantitative assessment of this point, the power spectral density of the backscatter return depth averaged between 10 and 15 m ($\langle\sigma\rangle_{10-15\ m}$) was calculated through the oscillatory tail sections (Figure 6a, black line). The peak in power occurs at 56 m (Figure 6b), and while there is some energy at large wavelengths, the cutoff is sharp at smaller length scales. This wavelength agrees well with those predicted by the resonance condition, $c'_2 = c_1$. Using ρ_0 and u_0 from the second profiling series, the predicted wavelength is almost identical to the observed wavelength (Figure 6c).

[26] If field conditions were uniform and stationary (as often employed in modeling and laboratory analyses), the evolving form of the leading wave would likely be attributed to dispersion, especially if the evolution occurred in an early wave stage. However, nature provides a complex and rich environment, and the response of the waveform to variations in density and velocity is not easily confined. For example, the observed surfacing of the mixed layer and contraction of the transition layer could have resulted in the "more" nonlinear waveform in the final series. The sudden appearance of the mode 1 waves could then be attributed to amplitude growth of a copropagating tail in response to increased nonlinearity in the mode 2 wave. Modeling studies have noted an analogous response as increased wave nonlinearity, which in these cases is set by amplitude, results in growth of oscillatory tails [*Stastna and Peltier*, 2005; *Williams and Wilson*, 1988]. The dominance of a single, short wavelength that agrees with the resonance condition further supports this mechanism for tail growth.
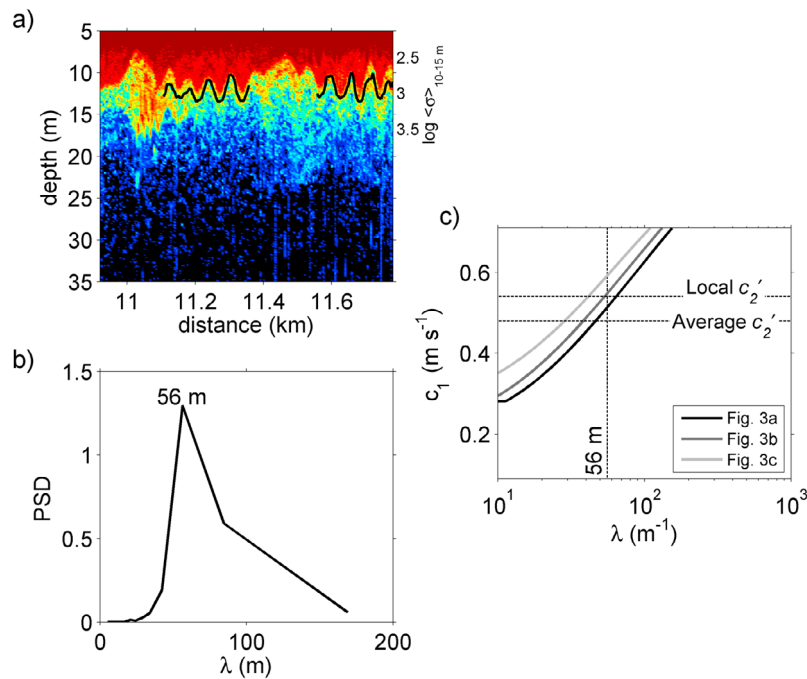
Figure 6. (a) Acoustic backscatter and (b) power spectral density of backscatter return averaged between 10 and 15 m. Wave tails were isolated (black overlay in Figure 6a) before spectra were calculated. (c) Mode 1 linear wave speed as a function of wavelength for the three profiling periods (Figures 3a–3c). Horizontal dashed lines represent the average mode 2 wave speed (0.48 m s^{-1}) and the measured speed between the second and third series (0.54 m s^{-1}).

[27] The group speed of the mode 1 waves, $c_1^g = \partial\omega/\partial k$, was calculated from the dispersion relation, $\omega(k)$, solved for using the TG equation. The value of c_1^g was approximately 0.3 m s^{-1} less than the linear phase speed. Taking the length of the mode 1 tail, L, to be the distance between the first and second mode 2 waves (i.e., assuming that only the mode 1 waves ahead of the second mode 2 wave originated from the first mode 2 wave), this difference results in a development time, $\tau = L(c_1 - c_1^g)^{-1}$, of approximately 15 min for the mode 1 tail. The development time τ is consistent with the sudden appearance of the waves within the 30 min required to make the return transect. Given this time frame, the lack of multiple wavelengths in the tail further discounts dispersion in favor of copropagation. We expect that at least some variation in wavelength should exist if dispersion was important, since even very short waves (20 m) that travel 0.2 m s^{-1} slower than the mode 2 speed would only lag the leading wave by 350 m in 30 min. However, regardless of the mechanism, the radiated wave tail contributes to the evolving energetics of the leading wave.

5. Energetics

5.1. Details of Energy Calculation

[28] While the profiling method allows for very fine resolution of the vertical structure (1 m), the horizontal resolution is unfortunately coarse. In order to calculate the available potential energy (APE) of the wave, the density structure was interpolated onto a finer horizontal grid (100 points per wave). Backscatter images were used to obtain a horizontal shape function both above and below the wave's

centerline. At each vertical level, a linear regression of the observed density displacements, η, onto these functions was used to fit the data onto the refined grid. After obtaining this high-resolution displacement field, the density is found by assuming $\rho(z + \eta) = \rho_0(z)$. This method of interpolation depends upon the assumption that water column scatterers follow isopycnals, and thus, it depends on the local properties of the fluid and plankton. In this case, the interpolated density field agrees well with the measured density at a given location.

[29] The interpolated density field and wave velocity were used to calculate the APE,

$$\text{APE} = \iint (\rho - \rho_*)gz\,\mathrm{d}x\mathrm{d}z,$$

and the kinetic energy (KE),

$$\text{KE} = \iint \frac{1}{2}\overline{\rho}(u_{\text{wave}}^2 + w_{\text{wave}}^2)\mathrm{d}x\mathrm{d}z,$$

in the lead waves. In the previous expressions, w_{wave} is the wave vertical velocity, $\overline{\rho}$ is the average density, and ρ_* is the reference density, defined by the state of minimum potential energy [*Winters et al.*, 1995; *Hebert*, 1998]. The wave horizontal velocity, u_{wave}, was calculated by subtracting $u_0(z)$ along interpolated isopycnals. The integration limits extend across the wavelength and over the entire water column. Evaluating the above expressions through the lead wave in each transect yields total energies, $E = \text{APE} + \text{KE}$, that decreased from 51 kJ m^{-1} in the first transect to 41 and
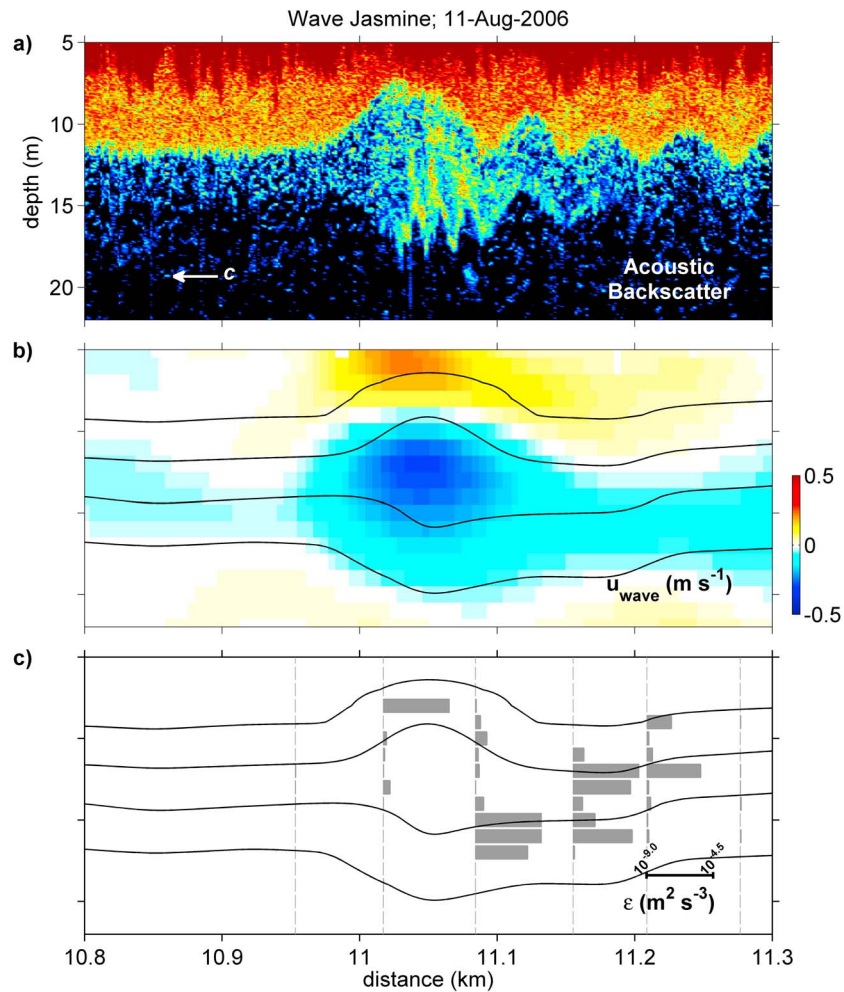
Figure 7. (a) Acoustic backscatter, (b) u_{wave}, and (c) measured dissipation through the leading wave of the third transect of Wave Jasmine.

33 kJ m^{-1} in the second and final transects, respectively. A schematic summarizing the lead wave energetics that are detailed in section 5.2 is represented in Figure 3 (right).

5.2. Dissipative Loss

[30] Approximately 35% of the leading wave's energy was lost between the first and third crossing, presumably to the combined effects of wave radiation and turbulent kinetic energy (TKE) dissipation, ϵ. Observations show elevated levels of TKE dissipation were present during the first and third transect (refer to Figure 7), increasing from background levels of between 10^{-8} and 10^{-7} m^2 s^{-3} up to 10^{-6} and 10^{-5} m^2 s^{-3} in the waves. While there was no observed increase in ϵ through the core of the lead wave during the second transect, the trailing mode 1 wave train that developed before the third crossing exhibited an average TKE dissipation slightly greater than 10^{-6} m^2 s^{-3}, over an order of magnitude larger than background levels. The average dissipative loss, D, through each wave was calculated by integrating the measured ϵ through the core of the lead wave (usually one profile) over the depth of the water column and then multiplying by the wavelength ($\lambda \times \int_0^H \overline{\rho}\epsilon dz$). Values of ϵ above 10 m depth are discarded because of contamination

by the ship wake. Dissipation due to bottom friction is assumed to be negligible; this assumption seems reasonable since (1) the water column is relatively deep (~100 m) and (2) wave velocities are small at the bottom.

[31] The resultant estimates of dissipative loss for the leading waves are 10 W m^{-1} in the first transect, 1 W m^{-1} in the second transect, and 20 W m^{-1} in the final transect. A sustained dissipative loss equal to the average of these three values (10 W m^{-1}) would deplete the leading wave's energy (51 kJ m^{-1}) in 1.5 h, corresponding to about $15T$ and a propagation distance of approximately 2.5 km (~15λ). While in reality turbulent mixing events are episodic in NLIWs, the high values of dissipation that were observed in two of the three profiling periods contributed to the short life span of Jasmine. These estimates of dissipative loss are comparable to typical values for the large-amplitude, long mode 1 waves observed during SW06.

[32] The observed loss in energy per unit time, $dE/dt = 3.5$ W m^{-1}, between the first and second crossing is roughly equal to the average dissipative loss (~5 W m^{-1}) between the first two transects. The change in energy ($\Delta E = 8$ kJ m^{-1}) between the second and final transects is approximately equal to that appearing in the trailing mode 1 waves,
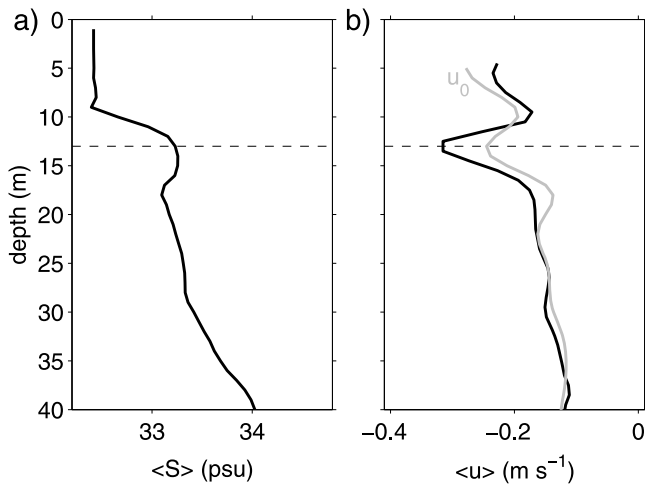
Figure 8. (a) Mean salinity profile and (b) velocity profile through the first wave of the third transect. For reference purposes u_0 is shown in grey.

$E_1 \approx 10$ kJ m^{-1}. This value was calculated by integrating the energy between the back edge of the leading mode 2 wave and the front edge of the second mode 2 wave. Energy loss to the radiated mode 1 tail was calculated as

$$D_1 = \frac{\mathrm{d}}{\mathrm{d}t} \int_z \int_x E_1^* \mathrm{d}x \mathrm{d}z = (c_1 - c_1^g) \times \int_z E_1^* \mathrm{d}z,$$

where E_1^*, the energy density of the mode 1 waves in units of J m^{-3}, is integrated over the water column. The above expression depends upon the relation $\mathrm{d}x = (c_1 - c_1^g)\mathrm{d}t$. This calculation results in an estimate of $D_1 \approx 10$ W m^{-1}; thus, the magnitude of energy loss to the mode 1 waves is comparable to the dissipative loss.

5.3. Comments on Wave Energetics

[33] To summarize, it appears that the initial mode 2 wave first loses energy to turbulent mixing and afterward loses a similar amount of energy to mode 1 wave radiation, assuming all waves between the first two mode 2 waves originated from the leading wave. The large dissipative loss at the third crossing and the assumed continued losses to wave radiation both likely contribute substantially to depletion of the mode 2 wave energy. The mixing associated with these waves may play an important role in eroding the barrier established by the pycnocline, especially considering their location centered in the transition layer. Thus, these waves, which have 10–100 times less energy than the mode 1 NLIWs observed in the same region, may have a disproportionate, localized effect on the coastal environment and the vertical fluxes of heat and nutrients. This is not dissimilar to open ocean internal waves, in which low modes carry the energy (over large distances) but high modes are associated with dissipation.

6. Discussion

[34] Wave Jasmine evolved quickly over the profiling periods, and the first transect was made after the mode 2

waves were clearly established. Similarly, mooring records are limited to analyses of preexisting mode 2 waveforms. Consequently, the formation mechanism was not directly observed and is not known for certain. Mooring- and ship-based observations of the mode 2 waves occur inshore of the shelf break over a gradually sloping bottom in a region where the larger mode 1 NLIWs were growing in amplitude; thus, generation by a breaking mode 1 wave as seen by *Helfrich and Melville* [1986] is unlikely. Given the steep, variable slope, mode 2 wave generation may be a result of tidal forcing near the shelf break, or wave formation may be tied to frontal intrusions as this region is characterized by a complex salinity-temperature field on the shelf. Below we speculate on these two generation pathways.

[35] The horizontally averaged salinity and velocity fields for Jasmine (Figure 8) show a complicated vertical structure, with an onshore pulse of relatively salty water located near the wave core. The horizontally averaged velocity (black line), which includes a contribution from the wave, mimics the reversal present in the background velocity (grey line), as if Jasmine is possibly "riding" along the shoreward propagating salty layer. Inshore at SW30, the mode 2 waves were classified into two types, the first of which was characterized by a salinity maximum in the vertical, similar to that exhibited by Jasmine. Six of the eight wave groups fit into this "type 1" category. In three of the six, the salinity maximums corresponded to the wave centerline (as shown in Figure 9a), and in the other three groups, salinity maximums were located slightly below the wave core. The temperature, salinity, across-shelf velocity, and vertical velocity for a wave group illustrating type 1 features are shown in Figure 9a. For this example, the mode 2 waves were near the front of a subsurface, shoreward pulse of high-salinity water. The vertical structure in salinity and velocity is reminiscent of the background conditions for Jasmine. The shear measured ahead of the wave was multilayered, and while near-surface temperature displacements were not completely resolved, the vertical velocity is mode 2 for the leading four waves.

[36] In contrast, the remaining two wave groups observed at SW30 showed no evidence of salinity intrusions (Figure 9b). For these waves (type 2), salinity was temporally stationary (neglecting high-frequency perturbations) for at least 2 h past the leading wave. The background velocity profile was near barotropic (at least below 10 m depth), and the temperature and salinity fields covaried. Limited conductivity measurements at SW29 prohibit classification of the final two mooring wave groups. The onshore appearance of the these two wave groups that cannot be tracked back to the offshore moorings points to an on-shelf process driving wave formation. And yet the lack of a subsurface, salty maximum for the type 2 waves, combined with the natural limitations in temporal and spatial resolution of the observations, prohibits an absolute answer to the formation question. However, regardless of whether intrusions directly force mode 2 waves, they likely help to erode the near-two-layer stratification that was seen regularly during this experiment, thus paving the way for creation of higher-mode waves. The mode 2 wave environment may have been particularly susceptible to these effects, as the 2006 experiment was preceded by a heat wave and intense rainfall, increasing the
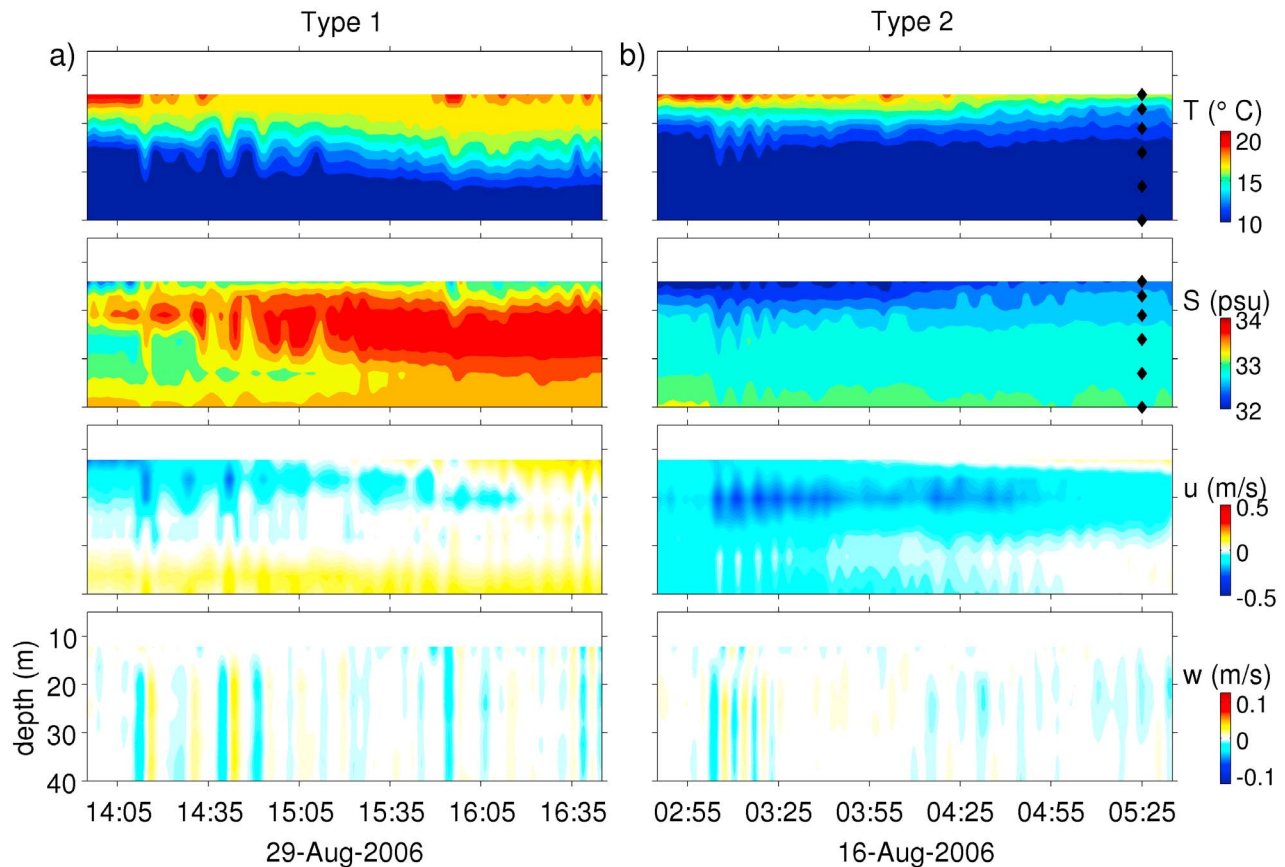
Figure 9. Contours of temperature, salinity, across-shelf velocity, and vertical velocity for (a) the third and (b) the seventh wave group recorded at SW30 (refer to Table 1).

stratification between the warm, fresh surface water and the cool, mixed water at depth.

7. Summary

[37] While the New Jersey nonlinear internal wavefield was dominated by mode 1 depression waves during the SW06 experiment, mode 2 waves were also present. The majority of mode 2 wave groups were observed in two midshelf mooring records that were 1 km apart near the 80 m isobath; two wave groups that were recorded at an inshore mooring near the 60 m isobath were not documented in the midshelf mooring records. All mode 2 waves propagated shoreward. The average amplitude was 4 m, and the average wave speed was 0.35 m s^{-1}. Waves occurred irregularly throughout the monthlong experiment.

[38] Detailed measurements obtained from the ship allowed for a more thorough analysis of the structure and energetics of one wave group. The vertical structure of the tracked mode 2 waves differed from linear theory, and the observed wave speed was slightly larger than the theoretical long mode 2 linear wave speed as expected for nonlinear waves. A mode 1, short-wavelength tail was observed to develop behind the leading mode 2 waves. The wavelength of the oscillations composing the tail was uniform and in agreement with that predicted for a copropagating tail. The energy loss calculated from shipboard measurements was

attributed to the radiation of the short mode 1 waves plus turbulent dissipation in the mixed layer. Mode 2 wave dissipation rates were comparable to large-amplitude mode 1 NLIW counterparts; however, energies were 10–100 times smaller. Consequently, the mode 2 decay time scale was much shorter (a few hours compared to tens of hours), and the propagation distance was smaller (a few kilometers compared to tens of kilometers).

[39] The inability to track mode 2 waves large distances through the mooring array and the rapid evolution of the ship-tracked wave group suggest that these waves are ephemeral in this variable shelf environment. The short-lived nature and comparatively subtle signatures of the waves may be a factor in the relatively few observations of these waves in the field, while, in reality, they could be numerous but difficult to observe. The formation of the mode 2 waves may be related to frontal intrusions, although the link is ambiguous. Nevertheless, frontal dynamics likely play a role in setting the stage for higher-mode waves by eroding the two-layer stratification present during much of the SW06 experiment. Although beyond the scope of this manuscript, questions surrounding the details of the mode 2 wave formation and the rapidly evolving structure of the ship-tracked wave could be further addressed using a numerical model. For example, it would be interesting to see if the somewhat subtle changes in background conditions initiate the growth of the mode 1 tail. Additionally,

exploring the consequences of complex shear fields to propagating mode 1 and mode 2 waves would be helpful in interpreting field observations.

References

Akylas, T., and R. Grimshaw (1992), Solitary internal waves with oscillatory tails, *J. Fluid Mech.*, *242*, 279–298.

Bogucki, D., L. G. Redekopp, and J. Barth (2005), Internal solitary waves in the Coastal Mixing and Optics 1996 experiment: Modal structure and resuspension, *J. Geophys. Res.*, *110*, C02024, doi:10.1029/2003JC002253.

Boyd, J. P. (1990), A numerical calculation of a weakly non-local solitary wave: The ϕ^4 breather, *Nonlinearity*, *3*, 177–179.

Davis, R. E., and A. Acrivos (1967), Solitary internal waves in deep water, *J. Fluid Mech.*, *29*, 593–607.

Duda, T. F., J. F. Lynch, J. D. Irish, R. C. Beardsley, S. R. Ramp, C.-S. Chiu, T. Y. Tang, and Y.-J. Yang (2004), Internal tide and nonlinear internal wave behavior at the continental slope in the northern South China Sea, *IEEE J. Oceanic Eng.*, *29*(4), 1105–1130.

Farmer, D. M., and J. D. Smith (1980), Tidal interaction of stratified flow with a sill in Knight Inlet, *Deep Sea Res., Part A*, *27*, 239–254.

Hebert, D. (1998), The available potential energy of an isolated feature, *J. Geophys. Res.*, *93*, 556–564.

Helfrich, K. R., and W. K. Melville (1986), On long nonlinear internal waves over slope-shelf topography, *J. Fluid Mech.*, *167*, 285–308.

Hunter, J. K., and J.-M. Vanden-Broeck (1983), Solitary and periodic gravity-capillary waves of finite amplitude, *J. Fluid Mech.*, *134*, 205–219, doi:10.1017/S0022112083003316.

Hüttemann, H., and K. Hutter (2001), Baroclinic solitary water waves in a two-layer system with diffuse interface, *Exp. Fluids*, *30*, 317–326.

Jackson, C. R. (2004), *An Atlas of Internal Solitary-Like Waves and Their Properties*, 2nd ed., Global Ocean Assoc., Alexandria, Va. (Available at www.internalwaveatlas.com)

Klymak, J. M., and J. N. Moum (2003), Internal solitary waves of elevation advancing on a shoaling shelf, *Geophys. Res. Lett.*, *30*(20), 2045, doi:10.1029/2003GL017706.

Kundu, P. K., and I. M. Cohen (2004), *Fluid Mechanics*, 3rd ed., chap. 12, 484–490 pp., Academic, San Diego, Calif.

Liu, A. K., Y. S. Chang, M.-K. Hsu, and N. K. Liang (1998), Evolution of nonlinear internal waves in the East and South China seas, *J. Geophys. Res.*, *103*, 7995–8008.

Maxworthy, T. (1980), On the formation of nonlinear internal waves from the gravitational collapse of mixed regions in two and three dimensions, *J. Fluid Mech.*, *96*, 47–64.

Mehta, A., B. Sutherland, and P. Kyba (2002), Interfacial gravity currents. II. Wave excitation, *Phys. Fluids*, *14*(10), 3558–3569.

Moum, J. N., and W. D. Smyth (2006), The pressure disturbance of a nonlinear internal wave train, *J. Fluid Mech.*, *558*, 153–177.

Moum, J. N., M. C. Gregg, R. C. Lien, and M. E. Carr (1995), Comparison of turbulence kinetic energy dissipation rate estimates from two ocean microstructure profilers, *J. Atmos. Oceanic Technol.*, *12*(2), 346–366.

Orr, M. H., and P. C. Mignerey (2003), Nonlinear internal waves in the South China Sea: Observation of the conversion of depression internal waves to elevation waves, *J. Geophys. Res.*, *108*(C3), 3064, doi:10.1029/2001JC001163.

Scotti, A., and J. Pineda (2004), Observation of very large and steep internal waves of elevation near the Massachusetts coast, *Geophys. Res. Lett.*, *31*, L22307, doi:10.1029/2004GL021052.

Stastna, M., and W. Peltier (2005), On the resonant generation of large-amplitude internal solitary waves and solitary-like waves, *J. Fluid Mech.*, *543*, 267–292.

Tang, D. J., et al. (2007), Shallow Water '06: A joint acoustic propagation/nonlinear internal wave physics experiment, *Oceanography*, *20*, 156–167.

Tung, K.-K., T. F. Chan, and T. Kubota (1982), Large amplitude internal waves of permanent form, *Stud. Appl. Math.*, *66*, 1–44.

Vanden-Broeck, J., and R. E. L. Turner (1992), Long periodic internal waves, *Phys. Fluids*, *4*(9), 1929–1935.

Vlasenko, V., and K. Hutter (2001), Generation of second mode solitary waves by the interaction of a first mode soliton with a sill, *Nonlinear Processes Geophys.*, *8*, 223–239.

Williams, G. P., and R. J. Wilson (1988), The stability and genesis of Rossby vortices, *J. Atmos. Sci.*, *45*(2), 207–241.

Winters, K., P. Lombard, J. Riley, and E. D'Asaro (1995), Available potential energy and mixing in density-stratified fluids, *J. Fluid Mech.*, *289*, 115–128.

Yang, Y. J., Y. C. Feng, M.-H. Chang, S. R. Ramp, C.-C. Kao, and T.-Y. Tang (2009), Observations of second baroclinic mode internal solitary waves on the continental slope of the northern South China Sea, *J. Geophys. Res.*, *114*, C10003, doi:10.1029/2009JC005318.

J. N. Moum and J. D. Nash, College of Oceanic and Atmospheric Sciences, Oregon State University, 104 Ocean Administration Bldg., Corvallis, OR 97331-5503, USA.

E. L. Shroyer, Woods Hole Oceanographic Institution, Clark 316A, MS21, Woods Hole, MA 02543, USA. (eshroyer@whoi.edu)